DIAGNOSIS AND OPTIMIZATION OF VEHICLE ROAD NOISE UTILIZING THE KRIGING SURROGATE MODEL

Zhijie HUANG[1,2], Haijun WANG[1,2,*] ,Zhengxin LAN[1*], Lei HE

A road noise diagnosis and optimization strategy based on the Kriging surrogate model is presented in this paper, aiming to elevate automobile NVH (Noise, Vibration, Harshness) performance. Utilizing the Transfer Path Analysis (TPA) method, the study initially identifies the critical paths for noise propagation. Design parameters pertaining to these paths are then designated as variables, with the overall vehicle road noise considered as the response function. Through the application of optimal Latin hypercube sampling, Design of Experiments (DOE) analysis is conducted, yielding variable and response data. Based on this, a Kriging surrogate model is constructed for road noise response. This model provides precise predictions of the objective function's reactions to shifts in design variables, subsequently minimizing computational load throughout the optimization process. A detailed quantitative assessment of the relationship between design variables and the objective function reveals the primary factors influencing road noise. Furthermore, a multi-objective genetic optimization algorithm is deployed to efficiently search for the global optimal solution aimed at minimizing road noise. This method has proven to be highly effective among numerous possibilities, significantly enhancing optimization efficiency and carrying substantial engineering significance for improving vehicle NVH performance.

Keywords: NVH, Transfer Path Analysis, Noise Optimization, Optimal Latin Hypercube, Kriging, Multi-Objective Genetic Optimization.

1. Introduction

Road noise refers to the medium- to low-frequency noise typically ranging from 20-300Hz generated inside a vehicle when random loads, caused by road irregularities, are transmitted through the tires to the chassis suspension and body, resulting in acoustic-structural coupling between the interior sound cavity and sheet metal components. It affects the riding comfort of the vehicle and is one of the NVH (Noise, Vibration, Harshness) performance aspects that consumers focus on when purchasing a vehicle, hence it receives significant attention from major automobile companies. Numerous scholars and experts have done extensive work on this. Bai Z[1] built a transfer path model with secondary contributions for an SUV to identify structural noise issues caused by vibrations in the cockpit and conducted load identification, determining the main excitation points and energy

[1] Liuzhou Railway Vocational and Technical College. Liuzhou, Guangxi, 545000, China
[2] Liuzhou Yingqin Tuolan Automobile Technology Co., Ltd. Liuzhou, Guangxi, 545000, China
*Corresponding Authors: Haijun WANG. Email: whjun69@sina.com； ZHENGXIN Lan. Email: 13877260072@163.com

characteristics causing interior noise along a certain path. Chen Zhao[2] proposed a Fast Systems (FS) vehicle road noise CAE diagnostic and optimization method, systematically outlining the basic approach to road noise diagnosis and optimization; Wei Y [3], Sohrabi S [4], Dooho L [5], and Ragasso J [6] used the transfer path analysis (TPA) to determine the main noise transmission paths and completed the corresponding noise optimization design. Ce L [7], Yixuan L [8], Ke C [9], and Kanghyun A [10], to overcome the inefficiency and high workload of traditional TPA, adopted the Operational Path Analysis with Exogeneous Inputs (OPAX) for targeted diagnostics and optimizations, improving noise issues. These research efforts have provided strong support for the overall vehicle NVH development.

The aforementioned literature, based on TPA analysis, focuses on the diagnostic techniques for road noise problems. However, the results of TPA analysis can only determine the transmission paths that contribute significantly to road noise but cannot further lock down the key design parameters on the transmission paths. The actual process of road noise optimization often relies on engineering experience or combines techniques such as Operating Deflection Shapes (ODS) and Grid Participation Analysis (GPA) to determine optimization plans by repeatedly modifying design parameters, which is not very efficient. When many variables are involved, it is difficult to consider the cross-effects between variables and find a globally optimal solution.

This paper, set against the backdrop of actual road noise project development, proposes a more systematic and efficient method for diagnosing and optimizing road noise.

Firstly, based on the results of NVH subjective evaluation, we utilized the LSM NVH testing system to conduct road noise testing on actual vehicles. Through this testing, we obtained sound pressure curves within the passenger compartment and successfully identified the frequency ranges that exceeded the standards. To further investigate the road noise issue, we constructed a high-precision CAE (Computer-Aided Engineering) model of the entire vehicle. To improve calculation efficiency, we ingeniously introduced super-element technology into the model, thereby significantly reducing the time required for a single calculation.

Next, we utilized this CAE model to conduct a Transfer Path Analysis (TPA), successfully identifying the key paths that significantly impact road noise results. On this basis, we carefully selected design parameters on these key paths that could potentially have a direct impact on road noise, using them as subsequent optimization variables.

To systematically study the relationship between these optimization variables and road noise, we employed the Latin Hypercube Method to discretize these variables and conducted a Design of Experiments (DOE) analysis within the

road noise CAE simulation model. Through this analysis, we obtained discrete values for road noise responses and optimization variables. To more intuitively understand this relationship, we utilized the Kriging method [31] to fit these discrete results into a mathematical response surface (i.e., surrogate model) describing the relationship between road noise and optimization variables.

Based on this surrogate model, we delved into the quantitative relationship between optimization variables and road noise and successfully identified the most critical variables affecting road noise. To find the optimal variable combination that reduces road noise peaks, we employed a genetic optimization algorithm for optimization [25-27]. Ultimately, in real-vehicle validation, we proved the effectiveness of this optimal variable combination. It not only significantly enhanced the vehicle's NVH performance but also greatly improved the efficiency of road noise optimization for the entire vehicle.

In summary, our research provides new ideas and methods for NVH development, possessing significant theoretical and practical value.

2. Description of the actual vehicle road noise problem

In subjective evaluations of road noise in a new energy vehicle, a distinct rum bling sound was noticeable in the rear of the passenger cabin, severely affecting the d riving and riding experience. as shown in Figure 1, acoustic microphones were place d in the rear passenger compartment seats, and a full-vehicle road noise test was cond ucted in order to obtain accurate rear road noise data.

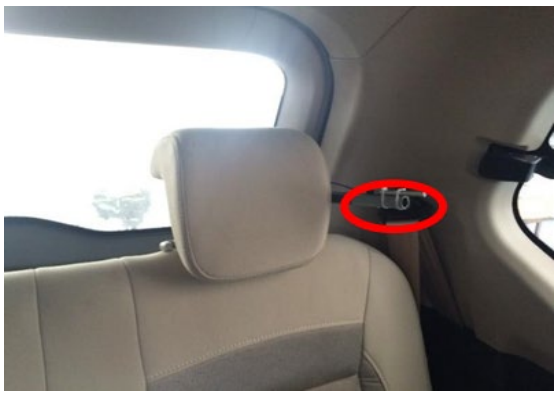

Fig. 1. Rear Passenger Compartment Microphone

The road noise test was carried out on the dedicated road noise track at the NVH testing facility for complete vehicles. The test vehicle was a self-developed new energy sedan with overall dimensions of 4835*1860*1515mm (length*width *height) and a curb weight of 1680kg. To ensure the accuracy and reproducibility of the test data, we avoided conducting tests on rainy days when the road surface was wet and slippery, and maintained the vehicle at a constant speed of 60km/h in

a straight line throughout the test. The NVH testing equipment from LMS (Laboratory for Measurement and Simulation) represents an industry-leading solution, widely applied in multiple fields such as automotive, aerospace, and military. This equipment includes high-precision, high-channel data acquisition systems that support multi-channel parallel real-time data acquisition, along with various sensors like accelerometers, microphones, force sensors, and pressure sensors, which collectively ensure precise capture of noise and vibration signals. Additionally, LMS offers a powerful software platform, LMS Test.Lab, which supports data acquisition, analysis, report generation, and can seamlessly integrate with other LMS software tools for a tight coupling of simulation and testing. These devices are characterized by high precision, high sampling rates, versatility, and portability, making them ideal for NVH testing of complete vehicles, NVH testing of components, and NVH optimization during the research and development process. In the experiments conducted for this paper, LMS equipment was utilized, with specific parameters outlined in Table 1.

Table 1

Test Equipment Parameter Table

Instrument Name	Performance,application, or requirements	Model number	Quantity
LMS SCADAS Data Acquisition System	Used for collecting and recording electrical signals generated by sensors, and completing the transformation of electrical signals into physical signals	Mobile 05	1
LMS Test and Analysis System Software	Used for data collection and analysis	LMS Test Lab.14A	1
1/4" PCB Microphone	Type 1 Sound Level Meter complying with GB/T 3785-1983 Frequency Range: 20 Hz to 20 kHz	130E21	4
PCB Three-axis Vibration Accelerometer	Mass: <10 grams Frequency Range: 2 Hz to 1000 Hz Frequency Response Error: ≤ ±5%	356A02	16
GPS Vehicle Speed Sensor	Measure vehicle speed		1

After applying A-weighting to the road noise test data, and combining subjective evaluations with the development experience of multiple vehicle models, it is generally observed that frequency bands where the road noise test curve exceeds 50dB(A) often lead to customer complaints and grievances. The test results for this occasion, as shown in Fig. 2, reveal that in the frequency bands of 80-110Hz, 140-160Hz, and 200-210Hz, the road noise curve surpasses the 50dB(A) threshold. Notably, in the 140-160Hz band, the peak reaches as high as 63dB(A), which has become a crucial factor contributing to the rumbling noise in the rear of this vehicle model.

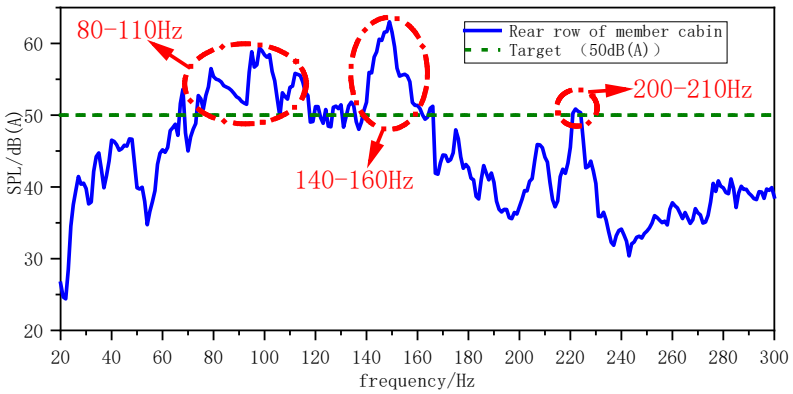

Fig. 2. Measured Road Noise Sound Pressure Level Curve

3. Whole vehicle road noise CAE simulation

Road noise is a vibro-acoustic coupling problem. Its governing equation is[32]:

$$\begin{cases} (K_s + j\omega C_s - \omega^2 M_s)u_i + K_c p_i = F_{si} \\ (K_a + j\omega C_a - \omega^2 M_a)p_i - \omega^2 M_c u_i = F_{ai} \end{cases} \tag{1}$$

where K, C, M, F represent the stiffness matrix, damping matrix, mass matrix, and load vector, respectively, with subscripts s and a denoting structural and acoustic quantities. In road noise analysis, the acoustic load in Equation (1) is relatively small and can be neglected, whereas the structural load originates from the hubs of the four wheels (hereinafter referred to as hub loads). Once the hub load matrix is obtained, the sound pressure level p_i can be determined through Equation (1). Unfortunately, due to structural constraints, we cannot directly measure the corresponding loads by placing mechanical sensors at the wheel hubs. Instead, we need to obtain the hub load vector by solving the inverse matrix[11].

To obtain the wheel hub input force, four accelerometers were installed at different positions on the steering knuckle of the test vehicle. During the whole vehicle road noise test conditions, the corresponding acceleration signals were measured as shown in Figure 3.

The input loads for CAE analysis, i.e., the hub excitations, are obtained via the inverse matrix method [12]

$$\mathbf{G_F} = \mathbf{H_A}^{+}\mathbf{G_A}\mathbf{H_A}^{+H} \tag{2}$$

where $\mathbf{G_F}$ is the hub load power spectrum matrix; $\mathbf{G_A}$ is the acceleration power spectrum matrix; $\mathbf{H_A}$ represents the transfer function matrix from wheel hub excitation to the acceleration response point, which is obtained through CAE analysis.

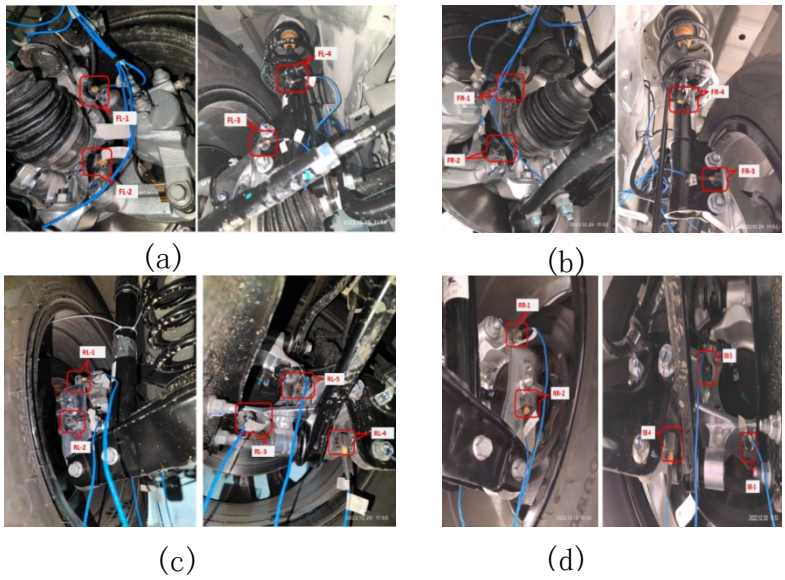

Fig. 3. Steering Knuckle Sensor Layout: (a) Left Front Wheel; (b) Right Front Wheel; (c) Left Rear Wheel; (d) Right Rear Wheel

The whole vehicle road noise CAE analysis model includes the chassis suspension system, power transmission system, interior body system, and the internal sound cavity model. Based on the hub excitation method, the input loads obtained through equation (5) already include tire information, hence the CAE model should exclude the tire model. Due to the large size of the model, the analysis time for a single run is long, but can be reduced using super element technology [13-15]. Based on the condensation characteristics of the super-element model, the division of super-elements should follow the following principles: the reduced structure of the super-element should possess a certain degree of independence, facilitating its separation from the remaining structure, thereby achieving the goal of reducing the solution scale. The interior body and acoustic cavity model exhibit a certain independence within the overall vehicle structure, primarily connected to the chassis and powertrain through bushings and bolts, which aligns with this principle and allows them to be condensed into super-elements. This paper generates super elements for the body and internal sound cavity model, as shown in Figure 4.

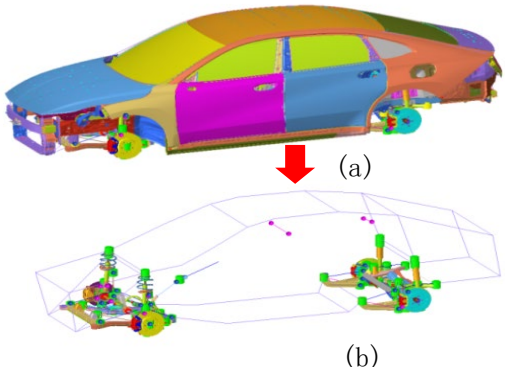

Fig. 4. Road Noise CAE Model: (a) Full Vehicle Model; (b) Reduced Super-Element Model

Due to the considered noise frequency range being 20-300Hz, in order to enhance the calculation accuracy of the super-element condensation model, when setting the modal extraction range for the interior body and fluid acoustic cavity model, the upper limit of the modal frequency extraction range is set to 1.5 times the upper limit of the calculation frequency (300Hz), which is 450Hz.this super element model reduces the time for a single simulation from 2.5 hours to 13 minutes while ensuring sufficient computational accuracy. Finally, the comparison between the road noise simulation and actual measurements is shown in Figure 5:

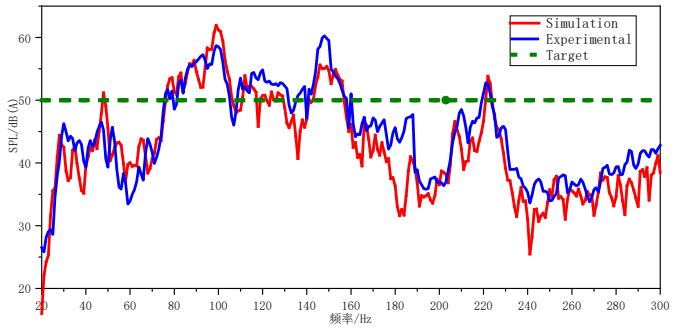

Fig. 5. Comparison of Road Noise CAE Analysis and Actual Measurements

The red line represents the road noise simulation curve, and the blue line represents the road noise test curve. It can be seen that the overall trend of the CAE simulation results matches the actual measurements, and the frequency ranges of the road noise problems are the same. The accuracy of this CAE model is high and can be used for subsequent optimization.

4. Road noise response kriging surrogate model

4.1 Definition of optimization variables

To pinpoint the primary transmission paths of road noise issues, the Altair NVH Director software was employed to conduct a whole vehicle road noise

Transfer Path Analysis (TPA) using the aforementioned CAE model. The vibrational energy causing road noise is transmitted into the interior acoustic cavity of the vehicle through the attachment points between the chassis and the body. Therefore, these chassis attachment points were defined as the transmission paths. The TPA analysis calculates and ranks the contribution of each path to the overall vehicle noise, thereby identifying the path with the greatest contribution. The analysis results are presented in Figure 6. The results indicated that the attachment points of the various control arms of the rear suspension (upper arm, lower arm, cross arm) contributed up to 97% to the overall vehicle road noise, with the largest contribution coming from the lateral direction of the rear cross arm, accounting for 28.4%.

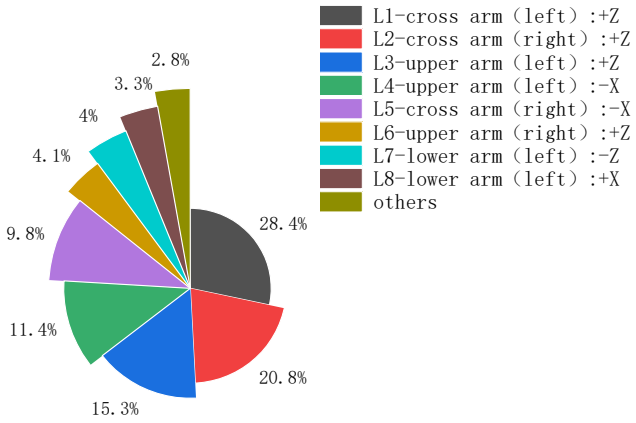

Fig. 6. Distribution of Path Contributions in TPA Analysis

It is evident that the transmission paths with the largest contributions share a common characteristic: these rear suspension control arm mounting points are all located on the rear subframe. This indicates that a significant portion of the vibrational energy causing road noise is transmitted from the rear subframe to the interior acoustic cavity of the vehicle. Therefore, there exists a design flaw in the rear subframe of this vehicle model. It is necessary to prioritize the optimization of the relevant design parameters of the rear subframe as variables for road noise response.

Based on the results of road noise analyses conducted on multiple vehicle models developed, the main design parameters of the rear subframe that significantly affect road noise performance are: the stiffness of the mounting point bushings, the thickness of the sheet metal, and the parameters related to the shape variations of the beams. However, these are only quantitative analysis results, and there are currently no reported studies on the quantitative relationship between these design parameters and road noise. Therefore, this paper will focus on

studying the quantitative relationship between these parameters, which will be taken as design variables, and road noise.

Optimization variables for the stiffness of the rear subframe bushings are established as follows: F_Bush_R (front bushing radial stiffness), F_Bush_A (front bushing axial stiffness), R_Bush_R (rear bushing radial stiffness), and R_Bush_A (rear bushing axial stiffness). At the same time, variables for the thickness of each beam are established: F_Beam (front crossbeam), R_Beam (rear crossbeam), H_Beam (side beam, symmetrical on both sides), as shown in Fig. 7:

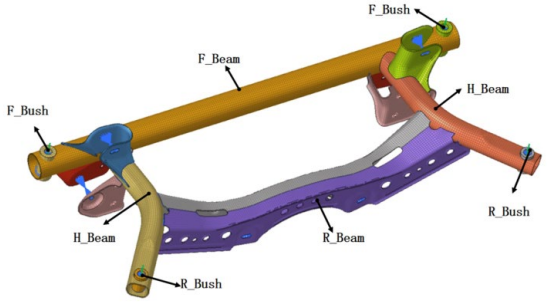

Fig. 7. Bushing stiffness variables and thickness variables

The shape variables for the beams are generated using the Hypermorph tool, subject to overall layout restrictions. The front and rear crossbeams can deform forwards and backwards (in the X-direction) and upwards and downwards (in the Z-direction), and the side beams can deform inward (in the Y-direction, symmetrical left and right), as shown in Fig. 8:

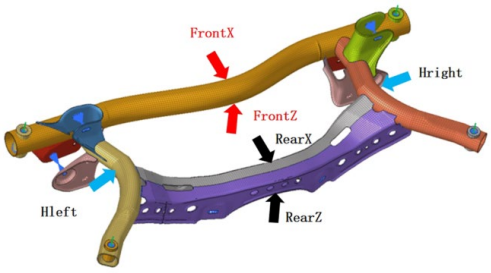

Fig. 8. Beam shape variables

Ultimately, for the 13 design parameters of the rear subframe, the following optimization variables were established, as shown in Table 2. It should be noted that the initial value of each parameter variable corresponds to the initial design state value of the vehicle model, while the upper and lower limits of the variables are based on the extreme values that can be achieved in the actual design of the design parameters.

Table 2

Design Variable Table

Variable	Lower limit	Initial value	Upper limit	Unit
F_Bush_R	5000	20000	21000	N/mm
F_Bush_A	400	20000	21000	N/mm
R_Bush_R	5000	20000	21000	N/mm
R_Bush_A	400	20000	21000	N/mm
F_Beam	1.5	2.2	2.8	mm
R_Beam	1.4	2	2.6	mm
H_Beam	1.8	2.5	3.2	mm
FrontX	-80	0	80	mm
FrontZ	-50	0	50	mm
rearX	-50	0	50	mm
rearZ	-50	0	50	mm
Hright	0	0	30	mm
Hleft	0	0	30	mm

4.2 Definition of response function

Based on the road noise simulation results, response functions for the frequency bands exceeding the standards are established using RMS-weighted methods:

$$R_{RMS} = \sqrt{\sum_{i=n_l}^{n_u} A_i^2 / (n_u - n_l)} \tag{3}$$

where n_l and n_u are the lower and upper limits of the exceeding frequency bands, respectively, and A_i is the A-weighted result of road noise pressure, given by:

$$\begin{cases} A_i = 20\log_{10}(A_f \cdot P_i / P_0) \\ A_f = 2.0 + \dfrac{12200^2 f^4}{(f^2+20.6^2)(f^2+12200^2)(f^2+107.7^2)(f^2+737.9^2)} \end{cases} \tag{4}$$

where P_i is the sound pressure value at the frequency point, $P_0 = 2.01\times10^5 P_a$ is the reference sound pressure; A_f is the narrow-band A-weighting coefficient, f is the narrow-band frequency[33]. Using equations (3) and (4), three road noise response functions for exceeding frequency bands were established: R_{100} (rear seat 80-110Hz), R_{150} (rear seat 140-160Hz), R_{205} (rear seat 200-210Hz).

4.3 Design of Experiments (DOE)

Although using super elements for road noise simulation saves time per simulation, multiple computations are still time-consuming. To improve the efficiency of diagnostics and optimization, this paper obtains sample point data through Design of Experiments (DOE), then constructs surrogate models and uses them for studying the correlation between design variables and responses, as well as for road noise optimization.

The experimental design requires an efficient sampling method; Optimal Latin Hypercube Sampling (OLHS) is a stratified sampling method that distributes sample points evenly across each dimension, ensuring coverage across the entire parameter space [16-18,31]. This method uses the maximum distance minimization criterion (Equation 5)[31], optimizing initial sample points through the simulated annealing algorithm, avoiding possible gaps, and enhancing sampling efficiency and quality.

$$\begin{cases} \min\limits_{i<j,j<n,i\neq j} \mathrm{d}(\mathrm{x}_i,\mathrm{x}_j) \\ \mathrm{d}(\mathrm{x}_i,\mathrm{x}_j) = d_{ij} = (\sum\limits_{k=1}^{m} \left| x_{ik} - x_{jk} \right|^2)^{1/2} \\ \rho_P = \min(\sum_{i=1}^{s} J_i d_i^{-2})^{1/2} \end{cases} \tag{5}$$

where d_{ij} is the distance between sample points. In this paper, a DOE analysis model is established in optimization software, and 500 instances of optimal Latin hypercube sampling were performed. Figure 9 shows the distribution statistics for FrontX (front crossbeam X-direction deformation parameter), from which the histogram and probability density function curve indicate that this sampling method achieves a uniform distribution of variables within the feasible domain.

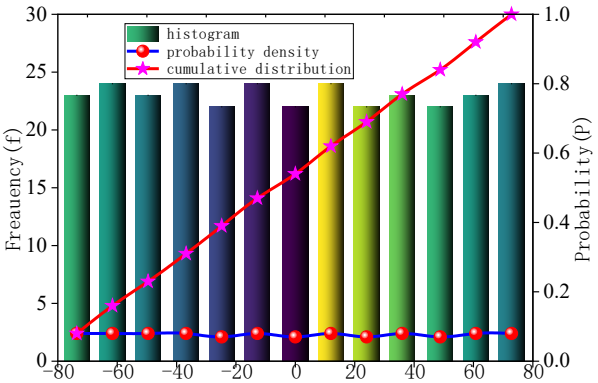

Fig. 9 Optimal Latin Hypercube Distribution of Typical Variables

4.4 Kriging-based whole vehicle road noise surrogate model

Due to its strong non-linear response description capability and the quantification ability for interpolation uncertainties, the Kriging surrogate model is widely used in the field of engineering optimization, achieving good optimization results in many complex engineering problems [19-24]. This model defines system response as a stochastic process, constructed by combining a polynomial regression model with a stochastic error[21]:

$$\begin{cases} \hat{f}(x) = f(x)^T \beta + z(x) \\ \varphi^2(x) = \sigma^2(1 + cRc - 2c^T r) \end{cases} \tag{6}$$

where β is a linear regression function; $f(x)$ is a polynomial function of the variables x, providing a good approximation for the model's establishment; σ^2 is the process variance; R is the correlation matrix of the variables x; r represents the correlation between sample points and prediction points; c provides the weights in the linear combination of the Kriging fitting model, which should be minimized. $z(x)$ is a non-zero covariance random process following a normal distribution $N(0,\sigma^2)$, providing a local approximation of the model bias. The covariance matrix of $z(x)$ can be written as[21]:

$$\begin{cases} E[z(\omega)z(x)] = \sigma^2\Psi(\theta,\omega,x) \\ \Psi(\theta,\omega,x) = \prod_{j=1}^{n}\Psi_j(\theta,\omega_j - x_j) \end{cases} \tag{7}$$

where $\Psi(\theta,\omega,x)$ is the spatial correlation function between any two sample points ω and x. The parameters θ in the correlation function are unknown and represent the correlation of samples across different spatial dimensions. n is the dimension of input parameters. In this paper, the correlation function uses the commonly applied Gaussian kernel function, as[21]:

$$\Psi_j(\theta,\omega_j - x_j) = \exp(-\theta_j \left|\omega_j - x_j\right|^2) \tag{8}$$

Kriging fitting was performed on the 500 sample data sets obtained in section C. The fitting accuracy of the three response functions was good, with Coefficient of Determination all exceeding 0.9 (the closer to 1.0, the higher the accuracy), as shown in Table 3.

Table 3

Kriging Surrogate Model Fitting Accuracy

Response Function	Corresponding Road Noise Frequency Band	Coefficient of Determination(R^2)
R_{100}	Rear Seat80-100Hz	0.928
R_{150}	Rear Seat140-160Hz	0.955
R_{205}	Rear Seat200-210Hz	0.932

5. Road noise diagnosis and optimization based on surrogate model

5.1 Correlation analysis between variables and road noise response

The Kriging surrogate model has established the mathematical relationship between road noise response and the variables. Utilizing this mathematical relationship, it becomes convenient to investigate the correlation between the variables and the road noise response. For the aforementioned thirteen variables, discrete values are taken at 100 points with equal intervals within their defined domains. Subsequently, combinations of these variables are substituted into the Kriging surrogate model to calculate the corresponding road noise responses. Finally, the Pearson correlation coefficients are computed:

$$r = \frac{\sum_{i=1}^{n}(x_i - \bar{x})(R_i - \bar{R})}{\sqrt{\sum_{i=1}^{n}(x_i - \bar{x})^2}\sqrt{\sum_{i=1}^{n}(R_i - \bar{R})^2}} \tag{9}$$

where x and R represent the variable and the response, respectively. Superscript- indicates its mean. Figure 10 presents the correlation coefficient matrix.From Figure 10, the following conclusions can be drawn:

The stiffness of the bushings has a strong correlation with road noise response. Specifically, the correlation coefficient between R_{100} and the axial stiffness of the front mounting point bushing reached 0.41, showing a strong positive correlation; whereas R_{150} and the axial stiffness of the rear mounting point bushing had a correlation coefficient as high as 0.52, becoming a key factor affecting road noise response. Notably, R_{205} shows a negative correlation with the axial stiffness of the front mounting point bushing, with a correlation coefficient of -0.46. These findings indicate that adjusting the stiffness of the rear subframe bushings has significant potential for road noise optimization.

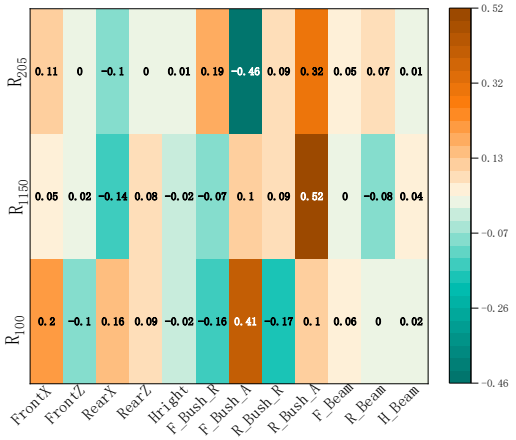

Fig. 10. Correlation Coefficient Diagram between Response Functions and Variables

Shape variables also correlate with road noise response, second only to bushing stiffness. For example, the correlation coefficients between R_{100} and the X-direction deformation of the front and rear crossbeams (FrontX, RearX) are 0.2 and 0.16, respectively, suggesting that optimizing related shape variables could reduce road noise response.

The thickness of the beams shows a smaller correlation with road noise response and may not be a focus for optimization.

5.2 Cumulative impact of multiple variables on road noise response

Based on the Kriging fitting results, response surface plots were generated, revealing that due to the cross-effects of variables, the road noise response within the feasible domain is very complex when influenced by multiple variables.

Figures 11(a) and (b) show the Gaussian smoothed surfaces for R_{150} within the domains of front and rear bushing stiffness, respectively, characterized by many peaks and valleys, indicating a highly complex response.

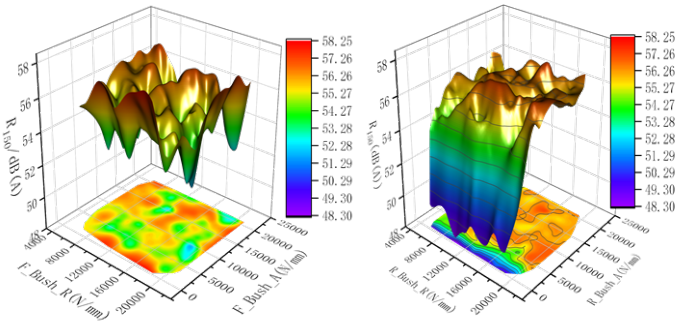

(a) (b)

Fig. 11. Response surface of R_{150} within the stiffness domain of the front and rear bushing: (a) Response surface of R_{150} within the stiffness domain of the front bushing; (b) Response surface of R_{150} within the stiffness domain of the rear bushing

5.3 Analysis of the impact of single variables on road noise response

To study the relationship between single variables and road noise, other variables can be fixed while conducting another DOE analysis using the Kriging surrogate model, and generating a second-level Kriging surrogate model with the sampled data.

5.3.1 Impact of bushing stiffness on road noise response

Taking the relationship between R_{100} and R_{150} and the rear bushing stiffness as an example, the response surfaces are plotted using a second-level Kriging surrogate model as shown in Figure 12:

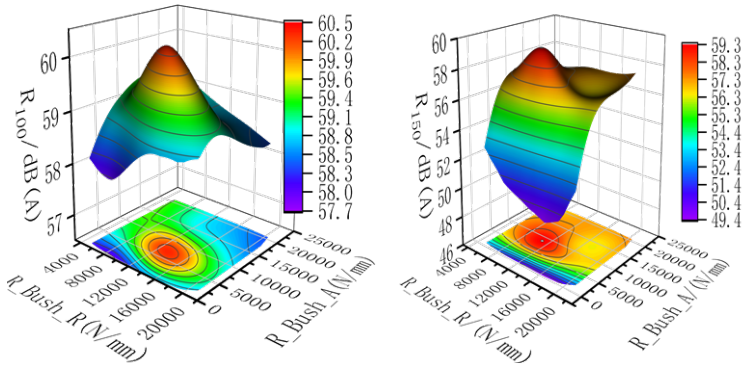

(a) (b)

Fig. 12. Impact of Rear Bushing Stiffness on R100 and R_{150}: (a) The effect of rear bushing stiffness on R_{100}; (b) The effect of rear bushing stiffness on R_{150}

Fig. 12(a) indicates that the road noise R_{100} peak is higher when the rear mounting point bushing stiffness is at 14000N/mm (radial) and 5000N/mm

(axial), and this combination should be avoided in the design. Figure 12(b) shows that as the axial stiffness of the rear bushing gradually decreases from 5000N/mm, the road noise R_{150} significantly reduces. This suggests that reducing the axial stiffness of the rear bushing, while ensuring its fatigue durability, can effectively reduce road noise in the 140-160Hz frequency band, providing a clear direction for optimization.

5.3.2 Impact of shape variables on road noise response

Figure 13 presents the response surfaces for R_{100} and R_{150} with the front crossbeam shape variables. It is observed that the greater the negative X-direction deformation of the front crossbeam, the smaller the responses of R_{100} and R_{150}. This indicates that the deformation of the front crossbeam of the rear subframe is beneficial for improving road noise performance.

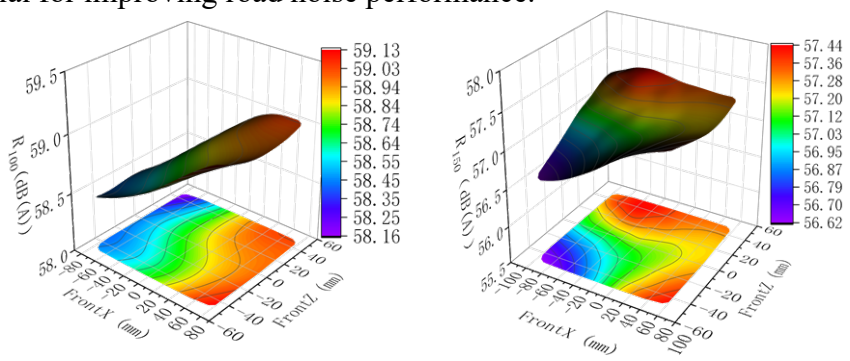

(a) (b)

Fig. 13. Impact of Front Crossbeam Shape Variables on R100 and R150: (a) The effect of the shape variable of the front crossbeam on R_{100}; (b) T The effect of the shape variable of the front crossbeam on R150

5.3.3 Impact of sheet metal thickness on road noise response

Fig. 14 shows the response surfaces for R_{100} and R_{150} with the thickness of the front and rear crossbeams' sheet metal. It can be seen that the response surface changes are moderate, which again indicates that the thickness of the beam sheet metal has a relatively minor impact on road noise response. Furthermore, the thickness of the front crossbeam has a positive correlation with road noise response; the greater the thickness, the greater the road noise response. Optimization should appropriately reduce the thickness to achieve lightweight goals.

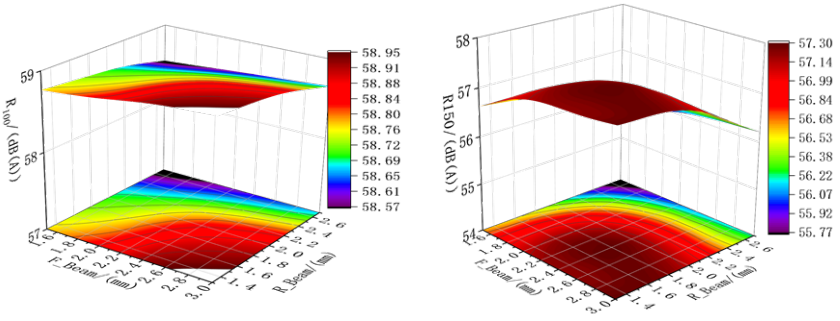

(a) (b)

Fig. 14. Impact of Front and Rear Crossbeam Sheet Metal Thickness on R100 and R150: (a) The effect of front and rear crossbeam thickness on R_{100}; (b) The effect of front and rear crossbeam thickness on R_{150}

5.4 Multi-objective genetic optimization of road noise response

Due to the complex and variable road noise response under the cumulative effect of multiple variables, traditional optimization algorithms tend to fall into numerical oscillations of local optima, making it difficult to achieve global optima [25-27]. This paper utilizes a multi-objective genetic optimization algorithm to optimize whole vehicle road noise.

The multi-objective genetic optimization algorithm is based on the basic framework of genetic algorithms, including population initialization, fitness assessment, selection, crossover, and mutation. It can evaluate the fitness of multiple objective functions, has a flexible selection mechanism for Pareto optimal solutions, and possesses better computational efficiency and global optimization capability.

The optimization mathematical model established in this paper is as follows:

$$\begin{cases} \min R(\mathrm{x})=\left[R_{100}(x), R_{150}(x), R_{205}(x)\right] \\ s.t. \\ x_L \le x \le x_U \end{cases} \tag{10}$$

where x represents the design variables, L and U represent the upper and lower limits, respectively. After 97 steps of optimization iteration (the iterative process curve is shown in Figure 15), the final global optimum solution is presented in Table 4.

From Table 4, it can be seen that the optimization of the whole vehicle road noise is significant. Particularly, the road noise in the 140-160Hz frequency range (R_{150}) has been significantly reduced by 13.2 dB (A). Comparatively, the road noise in the 80-110Hz (R_{100}) and 200-210Hz (R_{205}) frequency ranges, though not as significantly improved as R_{150}, have also achieved reductions of 3.3 dB(A)

and 0.6 dB(A), respectively, proving that the optimization strategy has a certain effect across multiple frequency bands.

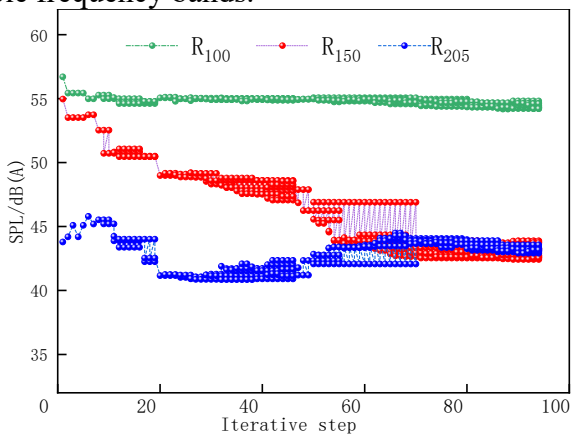

Fig. 15. Multi-objective Genetic Optimization Iterative Process

Table 4

Multi-objective Genetic Optimization Results for Road Noise

	Item	Initial Value	Optimized Value	Increment	Unit
Variable	FrontX	0	-80.0	-80	mm
	FrontZ	0	-41.0	-41	mm
	rearX	0	50.0	50	mm
	rearZ	0	-50.0	-50	mm
	Hright	0	20.4	20.4	mm
	Hleft	0	20.4	20.4	mm
	F_Bush_R	20000	13688	-6312	N/mm
	F_Bush_A	20000	570.0	-19430	N/mm
	R_Bush_R	20000	11115	-8885	N/mm
	R_Bush_A	20000	425	-19575	N/mm
	F_Beam	2.2	2.0	-0.2	mm
	R_Beam	2	2.5	0.5	mm
	H_Beam	2.5	2.0	-0.5	mm
Response	R_{100}	58.1	54.8	-3.3	dB(A)
	R_{150}	57.1	43.9	-13.2	dB(A)
	R_{205}	43.8	43.2	-0.6	dB(A)

To validate the feasibility of the optimization solution, manual samples of the subframe and bushings were made according to Table 3, and real vehicle validation and whole vehicle road noise curve tests were conducted. From Figure 16, it can be seen that the optimization solution is effective, with a noise reduction in the 140-160Hz frequency range exceeding 10 dB(A), significantly improving the whole vehicle's NVH performance.

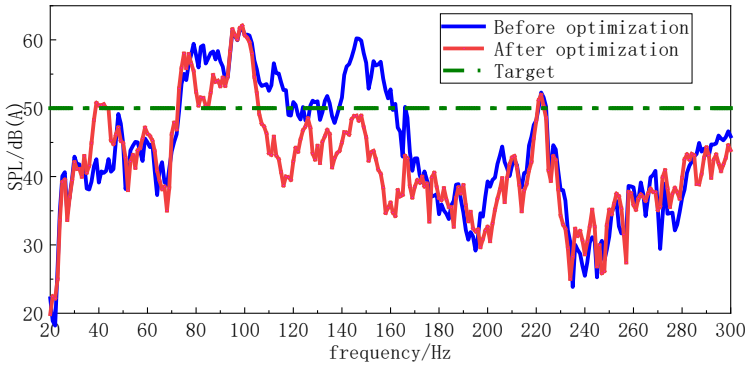

Fig. 16. Real Vehicle Validation of Whole Vehicle Road Noise Optimization

6. Conclusions

This paper, leveraging traditional TPA analysis, has successfully identified the primary paths for road noise transmission. Utilizing super-element technology alongside optimal Latin hypercube sampling, a Kriging surrogate model was generated. Through this surrogate model, an analysis of the correlation matrix between variables and response functions was conducted. Additionally, quantitative relationships between multiple and single variables pertaining to road noise response were examined. As a result, a comprehensive diagnosis of whole-vehicle road noise was achieved, precisely pinpointing the key variables that impact road noise. This approach offers novel insights for road noise diagnosis.

Considering that whole-vehicle road noise is influenced by multiple factors, and these factors exhibit significant cross-effects within their feasible domain, the optimization functions often possess numerous peaks and valleys. To tackle this complexity, the paper employs a multi-objective genetic optimization algorithm, emphasizing the pursuit of global optimal solutions. This method not only demonstrates computational efficiency but also possesses robust optimization capabilities.

Real-vehicle validation results indicate that the optimized solution has reduced whole-vehicle road noise response by 3.3 dB(A) in the critical frequency range of 90-110Hz and by 13.2 dB(A) in the 140-160Hz range. This significant reduction in noise levels has greatly enhanced the vehicle's NVH (Noise, Vibration, and Harshness) performance.

This research has shifted from the traditional development model primarily reliant on engineering experience and repetitive modifications, improving optimization efficiency and quality. The use of a Kriging surrogate model for whole vehicle road noise diagnosis and multi-objective genetic optimization provides new avenues for whole vehicle NVH development, with significant practical engineering implications. However, given that this study originated from an actual engineering project and was somewhat rushed, it employed older and more mature methods for the regression model and

optimization methods. In future research, more advanced regression strategies could be explored, such as combined surrogate models or deep neural network regression models, which could improve the accuracy of the surrogate model with fewer data sampling points. Similarly, for optimization algorithms, newly emerged and proven efficient intelligent optimization algorithms such as the Black-winged Kite Algorithm (BKA) [28] and the Differentiated Creative Search (DCS) [29] could be utilized to enhance optimization efficiency.

Acknowledgment

This study is supported by the National Natural Science Regional Foundation of China (Grant Number: 52065013) and the project of improving the basic scientific research ability of young and middle-aged teachers in colleges and universities in Guangxi (Grant Number: 2024KY1454, 2022KY1412)

R E F E R E N C E S

[1]. *Bai Z, Wei J, Chen K.,* Noise analysis of interior structure under powertrain excitation. Journal of Physics: Conference Series, 2024, 2691 (1).

[2]. *Chen Zhao, Huo Junyan, etc*. Application of vehicle road noise simulation and optimization technology. Noise and Vibration Control, 2019, 39 (03): 147151.

[3]. *Wei Y, Huazhong L, Jun C, et al.,* Turbo generator vibration source identification based on operational transfer path analysis technology. Journal of Vibro engineering, 2023, 25 (7): 1243-1256.

[4]. *Sohrabi S, Torres S A, Molins C E, et al*., A Comparative Study of a Hybrid Experimental–Statistical Energy Analysis Model with Advanced Transfer Path Analysis for Analyzing Interior Noise of a Tiltrotor Aircraft. Applied Sciences, 2023, 13 (22).

[5]. *Dooho L, Yeong Y P.,* Transfer path analysis using deep neural networks trained by measured operational responses. Journal of Mechanical Science and Technology, 2023, 37 (11): 5739-5750.

[6]. *Ragasso J, Helal M K, Moro L.,* Transfer-path analysis to estimate underwater radiated noise from onboard structure-borne sources. Applied Ocean Research, 2024, 147 103979.

[7]. *Ce L, Yi-Hao Z, Xiao-Zheng Z, et al*., Source contribution analysis of vehicle pass-by noise using a moving multi-band model based OPAX method. Measurement, 2023, 218.

[8]. *Yixuan L, Jijun L, Kaixiang L, et al.,* The vibration environment prediction method based on OPAX. Xibei Gongye Daxue Xuebao/Journal of Northwestern Polytechnical University, 2022, 40 (6): 1320-1326.

[9]. *Ke C, Xiaodong Z, Yubo L, et al*., An improved denoise method based on EEMD and optimal wavelet threshold for model building of OPAX. Proceedings of the Institution of Mechanical Engineers, Part D: Journal of Automobile Engineering, 2021, 235 (14): 3530-3544.

[10]. *Kanghyun A, Kwon S L.,* Identification of Influence of Cross Coupling on Transfer Path Analysis Based on OPAX and OTPA in a Dummy Car. International Journal of Automotive Technology, 2021, 22 (3): 771-778.

[11]. *Zeng Qingyi, Wang Haitao, Ji Lichao, et al.,* Analysis and optimization of vehicle road noise based on wheel center load. Noise and Vibration Control, 2020 P 40 (4): 183189.

[12]. *Cho B Y,* .Spindle Load Application for NVH CAE Models by Using Principal Vector Approach[C]//SAE World Congress.2006.

[13]. *Zhang S ,Dong C ,Zhang H , et al*., Analysis method of non-periodic CMC structure based on super-element [J]. Ceramics International, 2024, 50 (12): 21611-21618.

[14]. *Tallarico D, Hannema G, Miniaci M, et al*., Super element modelling of elastic metamaterials: Complex dispersive properties of three-dimensional structured beams and plates. Journal of Sound and Vibration, 2020, 484.

[15]. *E. B, M. S, B. A, et al.,* Super element reduction of substructures for sequential load calculations in Open FAST. Journal of Physics: Conference Series, 2020, 1452 012033-012033.
[16]. *Alexander N.,* Super element simulation technique of dynamics for large-size systems “base - reinforced concrete structures - metal structures”. verification and approbation. International Journal for Computational Civil and Structural Engineering, 2019, 15 (4): 123-132.
[17]. *Guosheng L, Jiawei Y, Zeping W, et al.,* A sequential optimal Latin hypercube design method using an efficient recursive permutation evolution algorithm. Engineering Optimization, 2024, 56 (2): 179-198.
[18]. *Adnan K ,Matt A ,R. C S , et al.,* Optimal sampling using Conditioned Latin Hypercube for digital soil mapping: An approach using Bhattacharyya distance. Geoderma, 2023, 439
[19]. *Koushyar K, Arne K, Fabian D.* Isovolumetric adaptations to space-filling design of experiments. Optimization and Engineering, 2022, 24 (2): 1267-1288.
[20]. *Meng Y, Zhang D, Shi B, et al.,* An active learning Kriging model with approximating parallel strategy for structural reliability analysis. Reliability Engineering and System Safety, 2024, 247 110098.
[21]. *Jie Z ,Genshen F ,Zilong W , et al*., Shape optimization of closed-box girder considering dynamic and aerodynamic effects on flutter: a CFD-enabled and Kriging surrogate-based strategy [J]. Engineering Applications of Computational Fluid Mechanics, 2023, 17 (1):
[22]. *Habibirad A, Baghani O, Hesameddini E, et al.,* A meshless method based on the modified moving Kriging interpolation for numerical solution of space-fractional diffusion equation. Engineering Analysis with Boundary Elements, 2024, 163 1-11.
[23]. *Han H, Suh J.* Spatial Prediction of Soil Contaminants Using a Hybrid Random Forest–Ordinary Kriging Model. Applied Sciences, 2024, 14 (4).
[24]. *Bright A, Eric A, Edmund T B.* Conceptual cost estimation of highway bid unit prices using ordinary kriging. International Journal of Construction Management, 2024, 24 (3): 351-360.
[25]. *An J, Lee H, Kim W C.*, Weight Minimization of Type 2 Composite Pressure Vessel for Fuel Cell Electric Vehicles Considering Mechanical Safety with Kriging Meta model. Machines, 2024, 12 (2).
[26]. *Shboul B, Zayed E M, Ashraf M W, et al.,* Energy and economic analysis of building integrated photovoltaic thermal system: Seasonal dynamic modeling assisted with machine learning-aided method and multi-objective genetic optimization. Alexandria Engineering Journal, 2024, 94 131-148.
[27]. *Sun W, Lin S, Zhang H, et al*., A reduced combustion mechanism of ammonia/diesel optimized with multi-objective genetic algorithm. Defence Technology, 2024, 34 187-200.
[28]. *Păun A M, Coandă G H, Mincă E, et al.,* Improved Multi-objective Genetic Algorithm Used to Optimizing Power Consumption of an Integrated System for Flexible Manufacturing [J]. Studies in Informatics and Control, 2024, 33 (1).
[29]. *Wang J, Wang W, Hu X, et al.,* Black-winged kite algorithm: a nature-inspired meta-heuristic for solving benchmark functions and engineering problems. Artificial Intelligence Review, 2024, 57(4): 1-53.
[30]. *Duankhan P, Sunat K, Chiewchanwattana S, et al*. The Differentiated Creative search (DCS): Leveraging Differentiated knowledge-acquisition and Creative realism to address complex optimization problems. Expert Systems with Applications, 2024: 123734.
[31]. *Gao Fengling, Wu Yuan, Bu Xiaobing, et al*. Tire Optimization Design Based on Vehicle Road Noise Performance Improvement [J]. Automotive Engineering, 2021, 43(01): 145-151. DOI: 10.19562/j.chinasae.qcgc.2021.01.019.
[32]. *Li Lijun, Li Hongyan, Gang Xianyue, et al.* Research and Application of Numerical Calculation Methods for Acoustic-Solid Coupling Systems [J]. Journal of Engineering Design, 2010, 17(06): 449-453.
[33]. GB/T 3785.1-2010. Electroacoustics - Sound Level Meters - Part 1: Specifications [S]. Beijing: Standards Press of China, 2010.